American Mineralogist, Volume 79, pages 250–260, 1994

^{25}Mg nuclear magnetic resonance spectroscopy of minerals and related inorganics: A survey study

K.J.D. MacKenzie, R. H. Meinhold

New Zealand Institute for Industrial Research and Development, P.O. Box 31-310, Lower Hutt, New Zealand

Abstract

The ^{25}Mg MAS NMR spectra of 18 minerals and related inorganic compounds are reported, including representative carbonates, hydroxides, 2:1 and 1:1 phyllosilicates, olivine, and pyroxene. Most of the spectra, which were acquired at 11.7 T and MAS speeds of about 20 kHz, show evidence of second-order quadrupolar line shapes, and all are influenced to a greater or lesser extent by base-line distortion effects. Various spectral processing methods that compensate for these base-line distortions are discussed.

Spectral simulations have enabled estimates to be made of the nuclear quadrupole coupling constants and electric field gradient tensor asymmetry parameters. In those minerals for which reliable simulations could be made and for which good structural data are also available, better correlations are found with structural parameters reflecting the angular distortion of the $^{[6]}$Mg site than with simple octahedral bond-length parameters.

Introduction

Because of its applicability to nuclei such as Si and Al, solid-state nuclear magnetic resonance spectroscopy with magic angle spinning (MAS NMR) has proved to be an invaluable technique for investigating minerals, glasses, and ceramics (for a comprehensive review, see Kirkpatrick, 1988). Other nuclei such as ^{17}O, ^{23}Na, ^{133}Cs, ^{11}B, and ^{31}P have also been utilized in structural and exchangeable cation studies of minerals (Kirkpatrick, 1988). The magnesium silicates constitute an important mineral group, which has so far only been amenable to systematic study by ^{29}Si MAS NMR. The feasibility of ^{25}Mg solid-state NMR has been reported on by Dupree and Smith (1988), who observed sharp MAS signals at 8.45 T in a limited number of compounds in which the Mg was in undistorted sites. The signals from brucite and two magnesium silicate samples were extremely broad and were recorded using a static echo pulse sequence (Dupree and Smith, 1988). These workers concluded that despite the 10% natural abundance of this spin-½ nucleus and the considerable second-order quadrupole broadening of the central transition by comparison with ^{27}Al, solid-state ^{25}Mg NMR studies could potentially provide useful information on minerals and inorganic solids. The present survey, undertaken using a higher field (11.7 T) and high spinning speeds (up to 20 kHz), reports the first ^{25}Mg MAS NMR spectra of the Mg representatives of the principal mineral classes and related inorganic compounds, addresses some of the experimental problems arising from probe ringdown and the recovery of weak signals from distorted base lines, and attempts to relate the spectral properties to the known crystallographic features of the compounds.

Experimental

The minerals and other compounds used in this study are listed in Table 1, which includes the origin and chemical constitution of each sample. The samples were characterized by X-ray diffraction and EDAX analysis, and only those of good crystallinity and essentially free of secondary phases were selected.

The MAS NMR spectra were collected at 11.7 T using a Varian Unity 500 spectrometer operating at 30.584 MHz, with a Doty 3.5-mm probe spinning at 20 kHz. A 60° pulse of 3 μs was used for solids, usually with a recycle delay of 0.1 s and a spectral width of 100 000 Hz. Longer recycle delays and wider spectral widths were tried in some cases. T_1 measurements using a saturating comb gave values of 0.03 ± 0.008, 0.207 ± 0.032, and 15.9 ± 1.0 s for magnesium sulfate solution, talc, and periclase, respectively. The weak ^{25}Mg signal precludes accurate T_1 measurements on low Mg samples. In minerals with paramagnetic impurities and large electric field gradients (EFGs) at the Mg site, T_1 would be expected to be much less than in MgO, as was found for talc (0.2 s). However, rapid pulsing could possibly bias the results toward ^{25}Mg in the vicinity of paramagnetic ions. For most of the spectra shown here, several hundred thousand transients were acquired, but, except in minerals of very low Mg content (typically a few percent) or with Mg in very distorted sites, useful spectra could be obtained with only a few thousand transients. After acquisition, the spectra were processed with a Gaussian line broadening of 300 Hz. All the ^{25}Mg peak positions are quoted with respect to a saturated solution of $MgSO_4$.

Procedures for processing ^{25}Mg spectra

The ^{25}Mg spectra of minerals with broad, weak lines tend to be dominated by spurious base-line roll effects generated by probe ringdown, acoustic ringing, pulse breakthrough, etc., at the low Larmor frequency. In order to alleviate these effects for the probe used in this work, data acquisition needed to be started about 100 μs after

0003–004X/94/0304–0250$02.00

TABLE 1. Minerals and materials included in this study

Phase	Locality	Source	Impurities	Chemical constitution
Periclase	—	synthetic	—	MgO
Brucite	—	synthetic, BDH	trace $MgCO_3$	$Mg(OH)_2$
Hydrotalcite	—	synthetic, Kyowa Co., lot 580	—	$Mg_5Al_3(OH)_{16}\cdot 1.5CO_3\cdot 3.6H_2O$
Magnesite	Clinton, British Columbia	UBC no. 2744	—	$MgCO_3$
Dolomite	Nelson, New Zealand	—	<0.5% Fe	$MgCa(CO_3)_2$
Talc	Three Springs, W. Australia	—	≈0.2% Fe	$Mg_6Si_8O_{20}(OH)_4$
Hectorite	—	synthetic, Laporte Ind. Ltd.	—	$[Mg_{5.3}Li_{0.6}]Si_8O_{20}(OH)_4Na_{0.9}\cdot nH_2O$
Saponite	Banat, Hungary	Smithsonian 121563	—	$Mg_6Si_{7.4}Al_{0.66}O_{20}(OH)_4(½Ca,Na)_{0.66}$
Chrysotile	Nelson, New Zealand	NZGS 4519	1.16% Fe	$Mg_3Si_2O_5(OH)_4$
Antigorite	Mikonui, New Zealand	NZGS 1123		$Mg_3Si_2O_5(OH)_4$
Phlogopite	Madagascar	W. C. Tennant	—	$K_2(Mg_{5.1}Fe^{2+}_{0.3})[Si_{5.1}Al_{2.1}Ti_{0.1}]O_{20}(OH)_4$
Palygorskite	Florida	NZGS 39189	trace quartz	$[Mg_{2.2}Al_{1.7}Fe^{3+}_{0.4}]Si_8O_{19.6}(OH)_{1.9}(OH_2)_{4.5}Ca_{0.4}$
Sepiolite	Vallecas, Spain		—	$[Mg_{7.6}Al_{0.46}]Si_{12.4}O_{30}(OH)_{1.8}(OH_2)_4\cdot 8H_2O\cdot K_{0.2}$
Montmorillonite	Mississippi		quartz	$[Al_2MgFe^{3+}](Si_{7.5}Al_{0.5})O_{20}(OH)_4(½Ca,K)_{0.7}$
Forsterite	—	chrysotile, heated 900 °C	—	Mg_2SiO_4
Enstatite	—	talc, heated 1300 °C	trace cristobalite	$MgSiO_3$

excitation. For some of the minerals studied here, that could be satisfactorily achieved by shifting to the left by eight points (at 10-μs intervals) the free induction decay (FID) acquired after a 20-μs period with the receiver off. The success or otherwise of this simple procedure can he judged by its effect on the shape and position of the resulting spectra; in some minerals, for example chrysotile, the spectrum is composed of at least two component lines that appear to have very different T_2^* time constants, causing substantially different signal decay behavior during ringdown. In such cases, the relative intensities of the spectral components change markedly with the number of points by which the FID is shifted to the left, necessitating an alternative processing procedure using linear prediction methods. This technique, which uses software included in the Unity system, involves the removal of 100 μs of data acquired after a 20-μs period with the receiver off, with the resulting FID being used to calculate the linear prediction coefficients and thus recovering the missing first 12 points after excitation. The resulting spectra are then compared with those produced by starting the back linear prediction at different points and with a polynomial base-line correction made of the spectrum produced with data acquired immediately after the receiver-off period. For consistency, all the spectra reported in this paper were processed using this linear prediction method. However, it is possible that in some instances, broad peaks observed near the main peak may still be an artifact arising from inadequate base-line correction.

In order to check processing methods, spectra of talc were analyzed, using a 5-mm probe and a composite pulse technique for reducing ringing effects (Zhang et al., 1990). A preacquisition delay of 30 μs gave some breakthrough, but the talc spectrum after normal Fourier transformation was very similar to the linear prediction spectrum from the standard Bloch decay MAS spectrum. The same spectrum shape was also obtained using different preacquisition delays prior to linear prediction, and with shorter pulse lengths.

RESULTS AND DISCUSSION

The MAS NMR spectra of the minerals are shown in Figures 1–3. The spectra of all these minerals are relatively similar, since in each case the Mg is in its preferred octahedral coordination. However, the octahedral sites can vary in their degree of distortion, giving rise to electric field gradient (EFG) effects that can alter the position and shape of the spectra.

In cases where the EFG effects cause the resonance from a single Mg site to be measurably split [as in brucite (Fig. 1A), hydrotalcite (Fig. 1B), and magnesite (Fig. 1D, 1E)], such spectra can be simulated by assuming appropriate values for the nuclear quadrupole coupling constant χ (defined as e^2qQ/h), the EFG tensor asymmetry parameter η, and a Gaussian line broadening. The spectral data for the present suite of minerals are presented in Table 2.

The observed spectrum of a typical well-resolved EFG line shape (hydrotalcite) is shown in Figure 4A, together with the corresponding spectrum simulated using the values of χ, η, and Gaussian line broadening listed in Table 2 (Fig. 4B). Comparison of the observed and simulated spectra then allows an estimate to be made of δ_0, the chemical shift corrected for EFG effects. However, where EFG effects are suspected but the peaks are broad and featureless, unique values for χ, η, and the Gaussian line broadening cannot be determined; in such cases the spectra can be acceptably simulated using a range of possible parameters up to maximum values of χ and η, after which noticeable line-shape effects appear; this procedure results in a range of possible values for δ_0. A typical example is shown in Figure 4C and 4D, in which the observed triangular line shape of antigorite (Fig. 4C) has been satisfactorily simulated using the values in Table 2 (Fig. 4D).

A third possibility that has been identified in some of these ^{25}Mg spectra is the apparent presence of two Mg sites, each with different T_2^* relaxation times, confirming the desirability of a linear prediction procedure to process

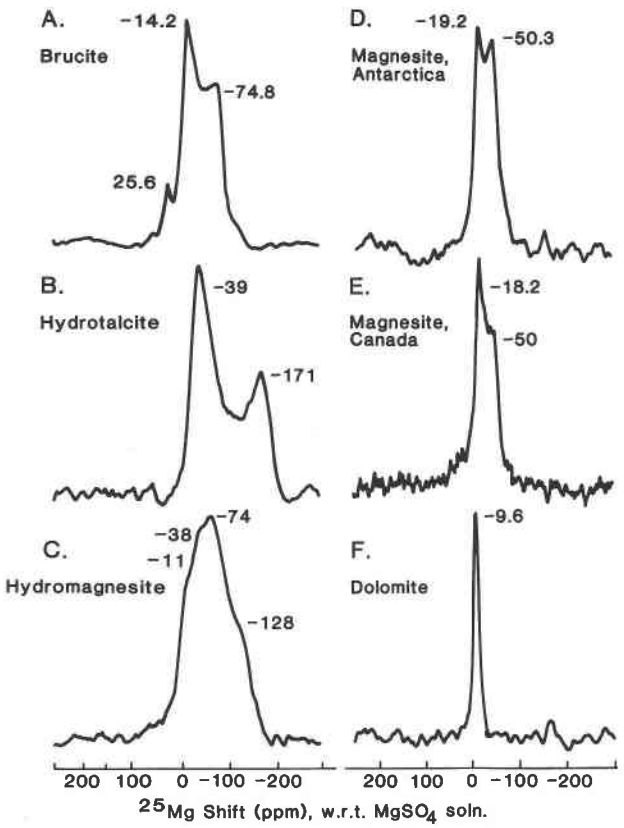

Fig. 1. (A–F) The ^{25}Mg MAS NMR 11.7-T spectra at room temperature of hydroxides, carbonates, and related minerals. Spinning speed 19.5–20 kHz, 300-Hz line broadening applied. Peak positions quoted with respect to saturated $MgSO_4$ solution.

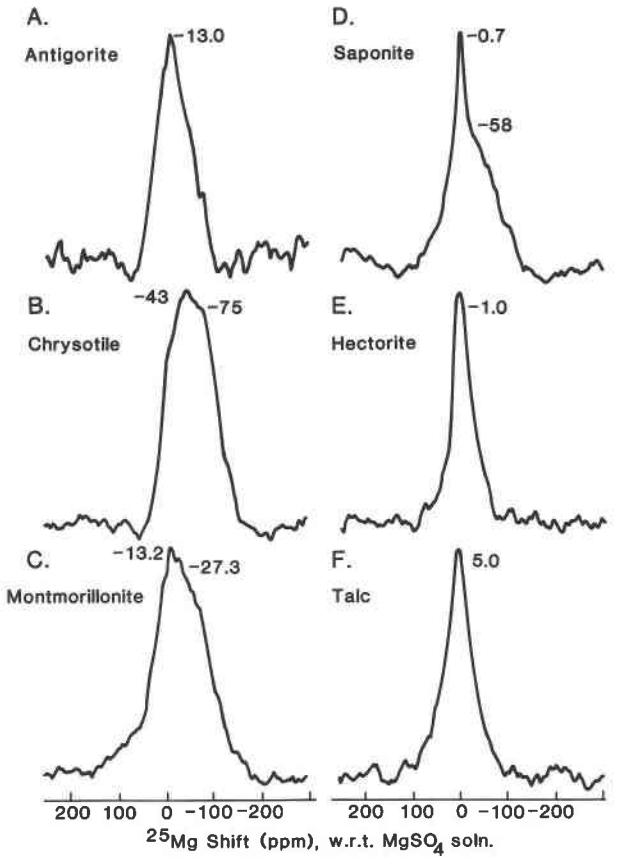

Fig. 2 (A–F) The ^{25}Mg MAS NMR 11.7-T spectra at room temperature of 1:1 and 2:1 layer silicates. Spinning speed 19.5–20 kHz, 300-Hz line broadening applied.

all the spectra. This T_2^* effect is most noticeable in the fibrous 1:1 layer silicate chrysotile (Fig. 2B) and the basic carbonate hydromagnesite (Fig. 1C), both of which contain two types of octahedral site. However, in chrysotile, these crystallographically distinct sites do not appear to correspond with the two sites of different T_2^*, which have relative populations considerably different from the approximately 1:1 ratio expected for the M1 and M2 sites. Furthermore, other examples of layer silicates containing M1 and M2 sites (montmorillonite, hectorite, saponite, talc) do not show these pronounced T_2^* effects; the significant differences in EFG experienced by these sites may therefore be affected by the mineral morphology, such as differences between surface and interior sites in the tubular fibrils of chrysotile. In the following discussion, *DI* is the angular distortion index for the octahedral site (Baur, 1974), defined and discussed later in this section.

Hydroxide and carbonate minerals

Brucite, $Mg(OH)_2$. The single $^{[6]}$Mg site in the brucite structure (Zigan and Rothbauer, 1967) is distorted from true octahedral symmetry, leading to the structural distortion parameters listed in Table 3. Spinning the sample at 20 kHz narrows the static spectrum and reveals a typical second-order quadrupolar line shape (Fig. 1A), which can be simulated using the values of nuclear quadrupole coupling constant χ, EFG tensor asymmetry parameter η, and Gaussian line broadening, which are listed in Table 2. These simulation parameters are similar to those deduced by Bastow (1991) in a study of single-crystal brucite. The additional low-intensity sharp resonance at 25.6 ppm is in the position expected for MgO (Fig. 3F) and may thus represent a small amount of decomposition product, but in a concentration too low to be detected by XRD.

Magnesite, $MgCO_3$. The spectra of five magnesite samples from various geographical locations have been obtained, of which two are shown here (Fig. 1D, 1E). The most typical spectrum is that of the Canadian magnesite (Fig. 1E), which is also found in samples from New Zealand and the former Czechoslovakia (MacKenzie and Meinhold, 1993a), but although of slightly different shape, the spectrum of Antarctic magnesite (Fig. 1D) is clearly closely related. The crystal structure of magnesite (Oh et al., 1973; Markgraf and Reeder, 1985) contains a single $^{[6]}$Mg site for which the *DI* and other distortion factors (Table 3) are satisfactorily similar when calculated from the structural data of both these authors. These structural

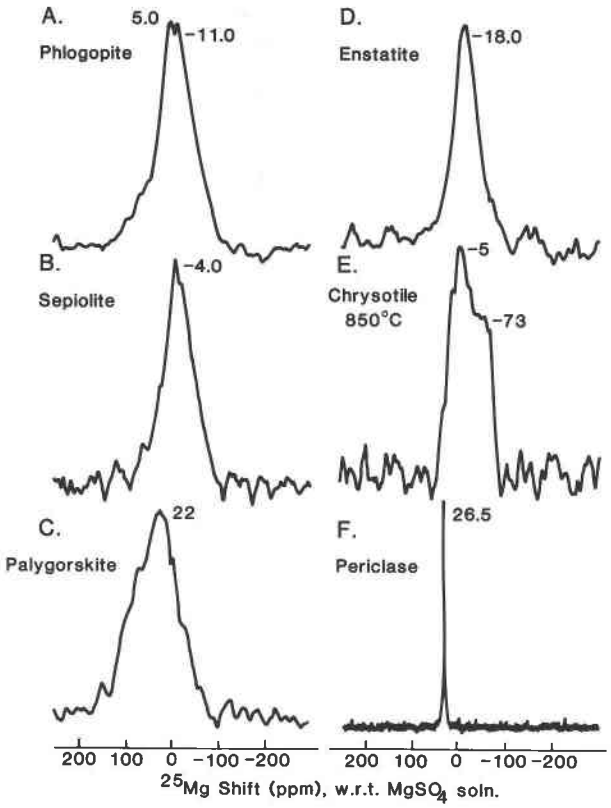

Fig. 3. (**A–F**) The ^{25}Mg MAS NMR 11.7-T spectra at room temperature of miscellaneous Mg-bearing minerals. Spinning speed 19.5–20 kHz, 300-Hz line broadening applied.

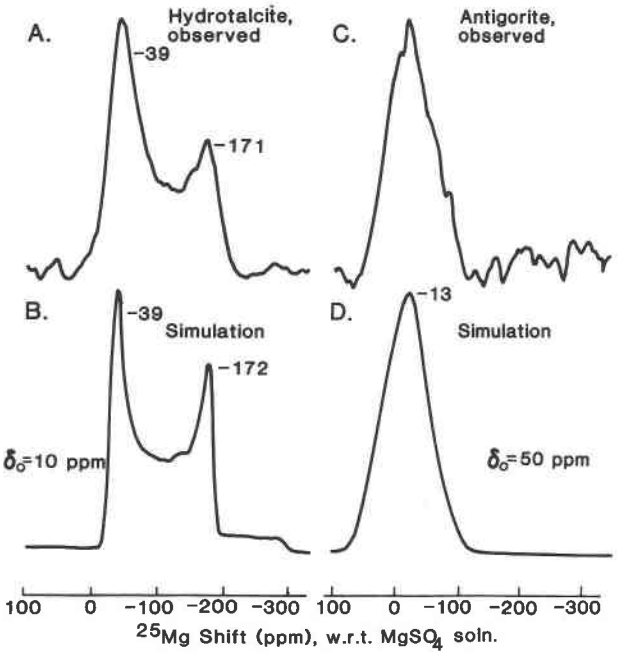

Fig. 4. Typical observed and simulated ^{25}Mg MAS NMR spectra. (**A** and **B**) Hydrotalcite; (**C** and **D**) antigorite.

parameters indicate that magnesite is considerably less distorted than brucite but more distorted than MgO. Both types of ^{25}Mg MAS NMR magnesite spectra can satisfactorily be simulated as quadrupolar line shapes using the parameters listed in Table 2, which indicate a slight difference between the values of χ and a nonzero value of η for the Antarctic sample. A much poorer simulation of the latter spectrum is obtained by setting $\eta = 0$, as required by the point symmetry of the Mg site in magnesite, suggesting that the structure of this sample may have undergone slight distortion, possibly by the incorporation of impurities or by the presence of defects.

Dolomite, $MgCa(CO_3)_2$. The crystal structure of dolomite (Reeder and Wenk, 1983) contains two octahedral cation sites of different distortion. The less distorted site ($DI = 0.019$) accommodates predominantly Mg, the more distorted site ($DI = 0.026$) containing predominantly Ca (Reeder and Wenk, 1983). The structural parameters of the less distorted Mg-containing site are listed in Table 3. The ^{25}Mg spectrum (Fig. 1F) is considerably narrower than that of magnesite and gives no indication of more than one Mg site. However, when plotted on an expanded scale, there is some evidence of quadrupolar structure, which becomes even more distinct when the sample is heated to 700 °C, below its thermal decomposition temperature (MacKenzie and Meinhold, 1993b). The spectral parameters are listed in Table 2.

Hydrotalcite, $Mg_6Al_3(OH)_{16}\cdot 1.5CO_3\cdot 3.6H_2O$. The structure of this mineral consists of brucite-like layers in which a proportion of the $^{[6]}$Mg is replaced by Al, the resulting charge imbalance being compensated for by the incorporation of CO_3^{2-} groups between the layers, in which region interlayer H_2O is also located (Allmann and Jepsen, 1969). The crystal structure determination was unable to distinguish between sites containing Mg and Al, a fact reflected by the mean octahedral *DI* listed in Table 3. The line shape of the ^{25}Mg spectrum spun at 20 kHz (Fig. 1B) is clearly quadrupolar and can be simulated using the values listed in Table 2 (Fig. 4B). Although the values of χ and line broadening are significantly greater for hydrotalcite than for brucite, the resulting value of δ_0 is not much different from that for brucite (or for Canadian magnesite).

Hydromagnesite, $Mg_5(CO_3)_4(OH)_2\cdot 4H_2O$. The structure of this mineral consists of a three-dimensional MgO_6 framework linked together by carbonate groups and containing coordinated OH and H_2O molecules (Akao et al., 1974). Two types of $^{[6]}$Mg site can be distinguished. The M1 octahedra form sheets running parallel to the [100] direction and are coordinated to four carbonate O atoms, one OH group, and one H_2O molecule. The M2 octahedra link these sheets together by sharing apices with the M1 octahedra and are coordinated to four carbonate O atoms and two OH groups. The M1 site is considerably more distorted than the M2 (Table 3). The ^{25}Mg spectrum (Fig. 1C) is broad and poorly resolved but contains shoulders that could arise from two doublets with different χ

Table 2. The ^{25}Mg spectral parameters for Mg-bearing minerals

Mineral	χ (MHz)	η	Line broadening (Hz)	δ_0 (ppm)	Width (Hz)	δ_{cog} (ppm)
Brucite	3.15	0	60	14.1	2270	−39
Magnesite, Canada	2.5	0	460	4.8	1310	−30
Magnesite, Antarctica	2.6	0.3	180	8.8	1350	−33
Dolomite	0.9	0	90	−4.3	160	−10
Hydrotalcite	4.4	0	400	10	4530	−70
Hydromagnesite M2	3.1	0	400	16	3620	−64
Hydromagnesite M1	3.6	0	400	−4		
Talc*	2.4	0.7	600	48	1540	5
Hectorite*	2.2	1.0	750	43	1140	−1
Saponite	0	0	400	0	400	−1
Montmorillonite	2.8	0	390	−4	3340	−20
	1.5	0	210	11		
Chrysotile					3190	−59
Antigorite*	2.9	0.7	1200	50	2270	−13
Phlogopite*	3.0	0.65	390–600	68	2210	−3
Sepiolite*	2.7	0.7	900	51	1780	−4
Palygorskite*	3.2	0.5	900	80	3210	22
Enstatite*	2.4	0.4	1050	27	1470	−18
Periclase	0	0	40	26.54	40	0
Forsterite M1**	4.996	0.963	305		2165	
Forsterite M2**	4.313	0.396	305		4422	

* Maximum value of χ and required line broadening, giving maximum δ_0. Values of χ could range down to 0, with large line broadening.
** Data from Derighetti et al. (1978).

values. By fitting Gaussian curves to the spectrum processed by linear prediction (Fig. 1C), the positions of these doublet components are found to be −11, −38, −74, and −128 ppm. These four spectral components are better resolved if the spectrum is processed using eight shifts to the left (Fig. 5, curve B) instead of the linear prediction method (Fig. 5, curve A). Figure 5 provides an example of a material in which the processing method can affect the shape and, to some degree, the resonance positions of a spectrum. Quadrupolar spectra for each of the two sites were simulated using all three possible combinations of doublet peaks, setting $\eta = 0$, and a Gaussian line broadening of 400 Hz. The parameters for the two most probable doublets (−11 with −74 ppm, −38 with −128 ppm) are shown in Table 2. The two simulated spectra for M1 and M2 (Fig. 5, curve D) can be combined in various ratios to give composite spectra with a range of relative intensities. The composite spectrum C shown in Figure 5 has been chosen as a reasonable approximation to the observed spectrum processed with eight shifts to the left (Fig. 5, curve B), but the relative intensities of the linear prediction spectrum (Fig. 5, curve A) are better approximated by combining the M1 and M2 simulated spectra with a more realistic assumption of approximately twice as many M1 as M2 sites.

The 2:1 layer magnesiosilicates

Talc, $Mg_6Si_8O_{20}(OH)_4$. Talc is a trioctahedral layer silicate with a structure consisting of two tetrahedral silicate sheets separated by an $^{[6]}$Mg-O(OH) sheet, the matching of the sheets being accomplished by a combination of slight flattening of the octahedra and a slight tilting of the

Table 3. Crystallographic distortion data for Mg-bearing minerals

Mineral	*DI*	$\Sigma \lvert\tan(\Theta_i - \Theta_m)\rvert$	$\frac{1}{6}\Sigma l_i$ (Å)	Reference
Brucite	0.076	1.452	2.102	Zigan and Rothbauer, 1967
Magnesite	0.019	0.383	2.105	Oh et al., 1973
Dolomite	0.019	0.36	2.084	Reeder and Wenk, 1983
Hydrotalcite	0.087	1.646	2.026	Allmann and Jepsen, 1969
Hydromagnesite M2	0.026	0.511	2.043	Akao et al., 1974
Hydromagnesite M1	0.065	1.18	2.097	Akao et al., 1974
Talc	0.056	1.027	2.069	Rayner and Brown, 1973
Montmorillonite	0.056	1.05	2.03	Tsipursky and Drits, 1984
Antigorite*	0.069	1.28	2.07	Mellini and Zanazzi, 1987
Phlogopite M1	0.065	1.26	2.063	Hazen and Burnham, 1973
Enstatite M1	0.048	0.914	2.079	Ohashi, 1984
Periclase	0	0	2.107	
Forsterite M1	0.087	1.557	2.101	Hazen, 1976
Forsterite M2	0.069	1.301	2.126	Hazen, 1976

* Data for 1*T* lizardite from Coli, Italy.

tetrahedra. There are two types of $^{[6]}$Mg site in the structure, the M1 sites, with OH groups at opposite corners of the octahedra, and M2 sites, with OH groups at adjacent corners (Rayner and Brown, 1973). The distortions of the M1 and M2 sites, calculated from the structural data of Rayner and Brown (1973) and from a more recent structure of Perdikatsis and Burzlaff (1981), have virtually identical values; the distortion parameters shown in Table 3 are based on Rayner and Brown (1973). The ^{25}Mg MAS NMR spectrum (Fig. 2F) shows a single unresolved resonance at 5 ppm, probably broadened by EFG effects. Although the featureless nature of this resonance militates against a satisfactorily unambiguous simulation, a reasonable approximation of the spectral shape can be obtained using the parameters listed in Table 2, which indicate large values of η and line broadening.

Hectorite, $[Mg_{5.3}Li_{0.6}]Si_8O_{20}(OH)_4Na_{0.9}\cdot nH_2O$. This trioctahedral layer lattice silicate is a member of the smectite group, but is structurally related to talc, by substitution of some of the $^{[6]}$Mg by Li, with charge balance provided by the exchangeable interlayer alkali cations. The present synthetic sample differs from natural hectorite in not containing small amounts of Al in the octahedral sites, but in all other respects (X-ray pattern, thermal reactions) it is similar to the natural mineral. The ^{25}Mg MAS NMR spectrum (Fig. 2E) is very similar to talc, suggesting that the Mg is not very sensitive to the presence of $^{[6]}$Li and vacancies. The featureless single unresolved resonance gives no suggestion of more than one Mg site, and the peak can be simulated in a number of ways, ranging from a non-EFG-broadened Gaussian peak (setting $\chi = 0$) to a maximum value for χ of 2.2 MHz, which, together with the values for the other parameters listed in Table 2, gives a maximum possible value for δ_0 fairly similar to that for talc.

Saponite, $Mg_6Si_{7.4}Al_{0.66}O_{20}(OH)_4(\frac{1}{2}Ca,Na)_{0.66}$. Saponite is another trioctahedral smectite, structurally related to talc by substitution in the tetrahedral sheets of Al for Si, with charge balance again being maintained by the presence of interlayer alkali or alkaline earth exchangeable cations. The ^{25}Mg MAS NMR spectrum (Fig. 2D) contains a single resonance similar to that of talc and hectorite, but apparently superimposed on a broader underlying hump. The appearance of this spectrum depends markedly on the method of processing; shifting to the left by 20 points leaves a single sharp line at 0 ppm, with a width of 110 Hz. As the number of points shifted to the left is reduced, and a base-line correction is applied, a broad component 4000–6000 Hz wide appears at about −30 ppm. Deconvolution of the spectrum obtained by linear prediction (Fig. 2D) (which is identical to the spectrum obtained with no shift to the left but a base-line correction) indicates that the broad component contains approximately 90% of the spectral intensity and appears somewhat similar to the spectrum of montmorillonite; it could, however possibly be due to a base-line artifact.

Montmorillonite, $[Al_2MgFe^{3+}](Si_{7.5}Al_{0.5})O_{20}(OH)_4(\frac{1}{2}Ca,K)_{0.7}$. Montmorillonite is a smectite in which the majority of

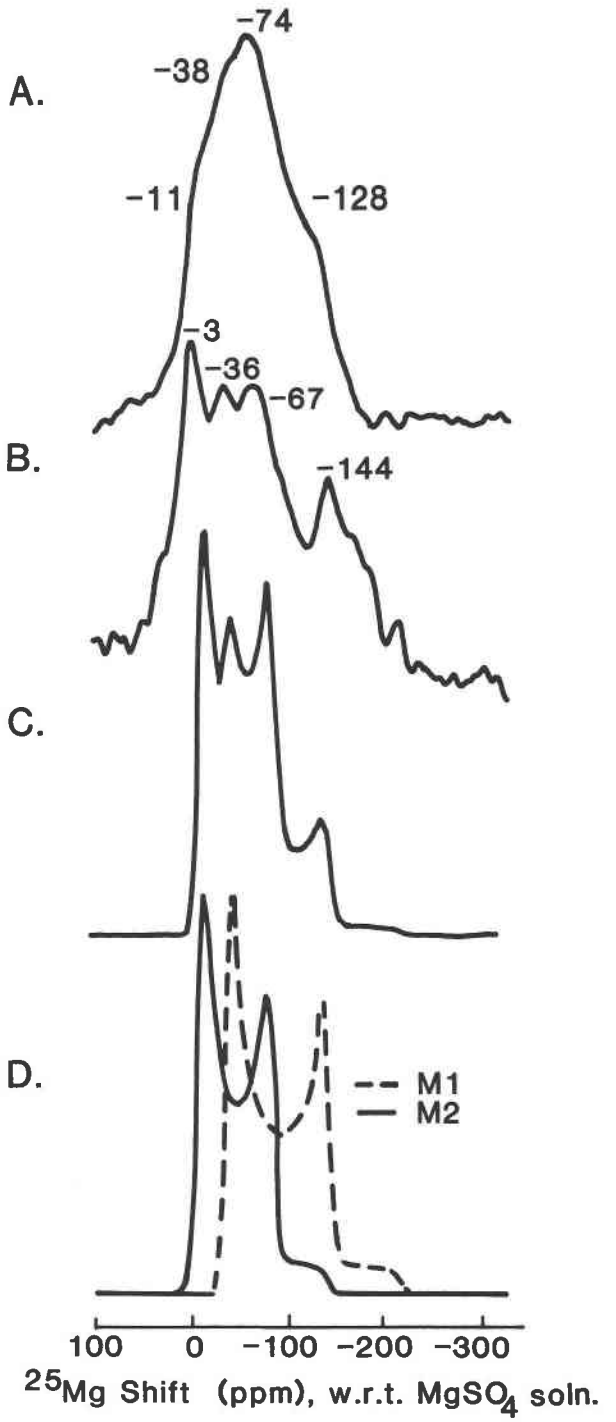

Fig. 5. (**A**) Observed ^{25}Mg MAS NMR spectrum of hydromagnesite, processed by linear prediction. (**B**) The same spectrum, processed with eight shifts to the left. (**C**) Addition of simulated M1 and M2 spectra in proportions 0.3M1 to 1.0M2. (**D**) Individual simulated M1 and M2 spectra.

the lattice substitution occurs in the octahedral sites, although limited substitution of $^{[4]}$Al for Si can also occur. This mineral is classified as a dioctahedral smectite, since the principal octahedral cation is Al, which can be replaced to varying degrees by Mg and other cations. The nature of these octahedral substitutions influences the structure of the mineral; oblique-texture electron diffraction studies by Tsipursky and Drits (1984) have identified three possible structural models, one in which all the trans octahedral sites are vacant, one in which both the cis and trans octahedral sites are equally populated, and one in which all the cations are randomly distributed over all the octahedral sites. Comparison of the chemical composition of the present montmorillonite with those examined by Tsipursky and Drits (1984) suggests that our sample is best described by the random cation distribution model, which was used as the basis for the montmorillonite structural parameters listed in Table 3. The ^{25}Mg spectrum (Fig. 2C) shows a broad peak at -13 ppm, with features at -27 and -74 ppm, and changes only slightly with processing method. Such a spectrum could arise from at least two sites with different EFGs. Thus, the observed shape can be described as a combination of two doublets, at -27 and -74 ppm and at 3 and -11 ppm. Such a spectrum can be simulated using the parameters of Table 2, but in view of the broadness and poor resolution of the spectrum, this procedure is too ambiguous to justify assigning doublets to specific sites, particularly since some additional intensity upfield may arise from another resonance of still higher EFG.

Phlogopite, $K_2(Mg_{5.1}Fe^{2+}_{0.3})[Si_{5.1}Al_{2.1}Ti_{0.1}]O_{20}(OH)_4$. Phlogopite is a trioctahedral member of the mica group, in which the major substitutions occur in the tetrahedral layer, with charge balance being provided by interlayer K^+. The octahedral sites in the present sample were shown by Mössbauer spectroscopy to accommodate the Fe^{2+}, in addition to Mg (our unpublished results). As in other 2:1 layer silicates, two octahedral sites (M1 and M2) can be distinguished in the crystal structure (Hazen and Burnham, 1973; Rayner, 1974); the crystal structures, however, indicate very similar angular distortions in the M1 and M2 sites, for which only the M1 value is listed in Table 3. On a long-range basis, the Fe^{2+} tends to be distributed randomly over M1 and M2 (Sanz and Stone, 1979). The ^{25}Mg MAS NMR spectrum (Fig. 3A) consists of a split peak, which can be simulated by a single-site quadrupolar line shape using the parameters listed in Table 2. However, such a simulation does not adequately account for the triangular shape of the base of this spectrum, which might be better described by a Lorentzian rather than Gaussian line shape, or alternatively by the presence of a broad underlying component or a base-line artifact.

The 1:1 layer magnesiosilicates

Chrysotile, $Mg_3Si_2O_5(OH)_4$. Chrysotile is the asbestiform modification of serpentine, in which the alternating Mg-O(OH) octahedral layers and Si-O tetrahedral layers are coiled into fibers along the **a** axis. This cylindrical structure introduces disorder along the circumferential (**b**) direction, permitting only two-dimensional X-ray structure determinations (Whittaker, 1956). Comparison of these partial structures with more recent complete structural determinations of the nonfibrous serpentine lizardite (Mellini, 1982; Mellini and Zanazzi, 1987) indicates strong similarities between the two structures (Wicks and O'Hanley, 1988) and suggests that the distortion of the octahedral site in lizardite might reasonably approximate that of chrysotile.

The ^{25}Mg MAS NMR spectrum of Nelson chrysotile (Fig. 2A), although broad, shows evidence of features that are also present in the spectrum of a Canadian (Cassiar) chrysotile (MacKenzie and Meinhold, 1994). Although both the Nelson and Cassiar peak shapes can be approximated by fitting Lorentzian lines at -90 and 8 ppm, with the Nelson sample requiring a third, broad component at about -22 ppm, the observed line shape is more likely to be second-order quadrupolar than Lorentzian. The shapes of the chrysotile spectra are extremely dependent on the processing method used to correct the FID for base-line effects introduced by probe ringdown, suggesting the presence of at least two components with different T_2^* time constants. By processing the spectra with a range of shifts to the left and fitting the component heights to a Lorentzian decay, T_2^* values of 58 and 315 μs are estimated for the components at about -90 and 8 ppm, respectively. This predicts Lorentzian line widths of about 5520 and 1010 Hz, respectively, for these spectral components, and that they occur in the ratio of about 9:1 to 16:1, suggesting that the different EFGs giving rise to them may be related to the fiber morphology.

Antigorite, $(Mg_{2.81}Fe^{2+}_{0.02}Fe^{3+}_{0.03})[Si_{1.95}Al_{0.05}]O_5(OH)_{3.68}$. Antigorite is a member of the serpentine group, in which the misfit between the octahedral and tetrahedral layers is overcome by curvature of the sheet in an undulating mode such that in each layer the structure can achieve the most efficient curvature in the (**a**) direction for misfit relief. Although only two-dimensional structural determinations have been made (Kunze, 1958), these indicate that the octahedral sheet is anomalously thick and that the a and b parameters are slightly larger than in lizardite. In the absence of a complete antigorite crystal structure determination, the DI for lizardite was taken as an approximation. The ^{25}Mg MAS NMR spectrum (Fig. 2A) is simpler than that of chrysotile in that it doesn't contain components of significantly different T_2^* and can be reasonably approximated by a second-order quadrupolar line shape using the parameters listed in Table 2 (Fig. 4D).

Other Mg-bearing minerals

Sepiolite, $[Mg_{7.6}Al_{0.46}]Si_{12.4}O_{30}(OH)_{1.8}(OH_2)_4 \cdot 8H_2O \cdot K_{0.2}$. The structures of sepiolite and palygorskite (see below) can both be regarded as variations of 2:1 phyllosilicates, since they consist of ribbons of 2:1 layer structure running along the **a** axis and linked together by alternate inversion of the SiO_2 tetrahedra. Thus, the tetrahedral layer is con-

tinuous, but the octahedral layer occurs on blocks, each one eight octahedral sites wide in sepiolite and five octahedral sites wide in palygorskite (Jones and Galan, 1988). In addition to the usual M1 and M2 octahedral sites as found in 2:1 phyllosilicates (the sites bonded to trans and cis OH groups, respectively), there is a third octahedral site, M3, at the edge of the octahedral ribbon and associated with two H_2O ligands. The remaining H_2O molecules and a small number of exchangeable cations occupy positions in the channels that run parallel to the chains. The trans M1 site is vacant, but precise details of the geometry of the other two octahedral sites are unknown. The ^{25}Mg MAS NMR spectrum (Fig. 3B) consists of a featureless triangular-shaped resonance, which is relatively uninfluenced by the processing method. The spectrum gives no indication of multiple sites and can be simulated satisfactorily by a single-site quadrupole line shape, using the parameters listed in Table 2.

Palygorskite, $[Mg_{2.2}Al_{1.7}Fe^{3+}_{0.4}]Si_8O_{19.6}(OH)_{1.9}(OH_2)_{4.5}$-$Ca_{0.4}$. The structure of this mineral is related to that of sepiolite, with full cation occupancy of the M2 and M3 octahedral sites and vacant M1 sites. Our ^{27}Al spectrum of this mineral confirms a recently reported ^{27}Al MAS NMR study (Guven et al., 1992), which indicates the presence of Al in octahedral sites only, and confirms that tetrahedral substitution is insignificant in this mineral (and probably in sepiolite also). The ^{25}Mg MAS NMR spectrum (Fig. 3C) displays a triangular-shaped resonance, somewhat broader than in sepiolite, but capable of satisfactory simulation by a single quadrupolar line shape with the maximum value of χ, which is listed together with the other parameters in Table 2. The resulting maximum value of δ_0 is the largest suggested for the present suite of minerals.

Enstatite, $MgSiO_3$. Enstatite is a pyroxene, containing the characteristic $(SiO_3)_n$ chains linked laterally by Mg. Of the three room-temperature polymorphs of enstatite, two (enstatite and orthoenstatite) are orthorhombic, and the third (clinoenstatite) is monoclinic. All polymorphs contain two Mg sites, namely, M1, which lies principally between the apices of the SiO_3 chains, and the larger and more distorted M2 site, which lies principally between the bases of chains. The crystal structure data for orthoenstatite (Morimoto and Koto, 1969; Ohashi, 1984) and for clinoenstatite (Ohashi, 1984) indicate very similar distortion indices for both polymorphs, for which only the less-distorted M1 site is listed in Table 3. The present sample, formed from talc heated to 1300 °C, has a ^{29}Si MAS NMR spectrum more characteristic of orthoenstatite (MacKenzie and Meinhold, in preparation). Its ^{25}Mg MAS NMR spectrum (Fig. 3D) contains a single resonance, which can be simulated by a single quadrupolar line shape with the parameters shown in Table 2. This resonance probably corresponds to Mg in the M1 site; the distortion in the M2 sites may broaden the Mg signal from these sites beyond detection.

Forsterite, Mg_2SiO_4. An attempt was made to determine the MAS NMR spectrum of forsterite derived from chrysotile by heating at 850 °C for 15 min, which, according to XRD and ^{29}Si MAS NMR, consists predominantly of crystalline forsterite. Although the resulting resonance had the appearance of a second-order quadrupolar line shape (Fig. 6, curve A), it represented only a few percent of the starting material and could have arisen from a Mg-containing impurity rather than from forsterite. The structure of forsterite, the Mg end-member of the olivine series, consists of a framework of individual SiO_4 tetrahedra pointing alternately up and down in both the **a** and **b** directions and linked by $^{[6]}$Mg, half of which are located at the centers of symmetry (the M1 sites) and half on the reflection planes (the M2 sites). Crystallographic

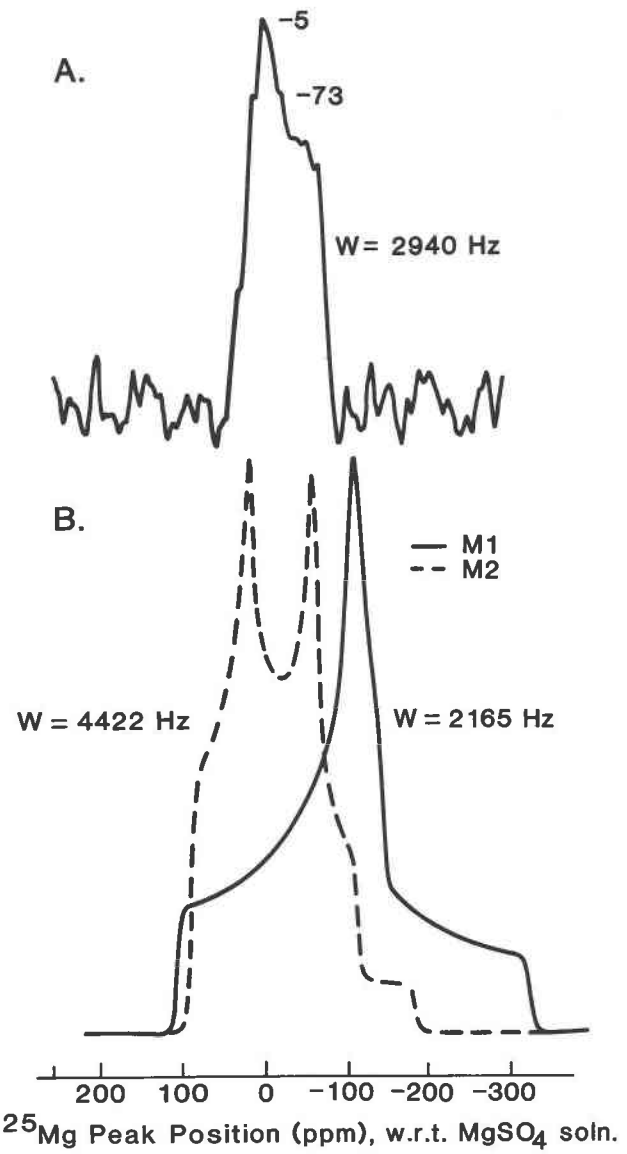

Fig. 6. (**A**) Observed spectrum from chrysotile, heated at 850 °C. *W* denotes full width at half height. (**B**) Spectra of the M1 and M2 sites of forsterite, simulated from the data of Derighetti et al. (1978).

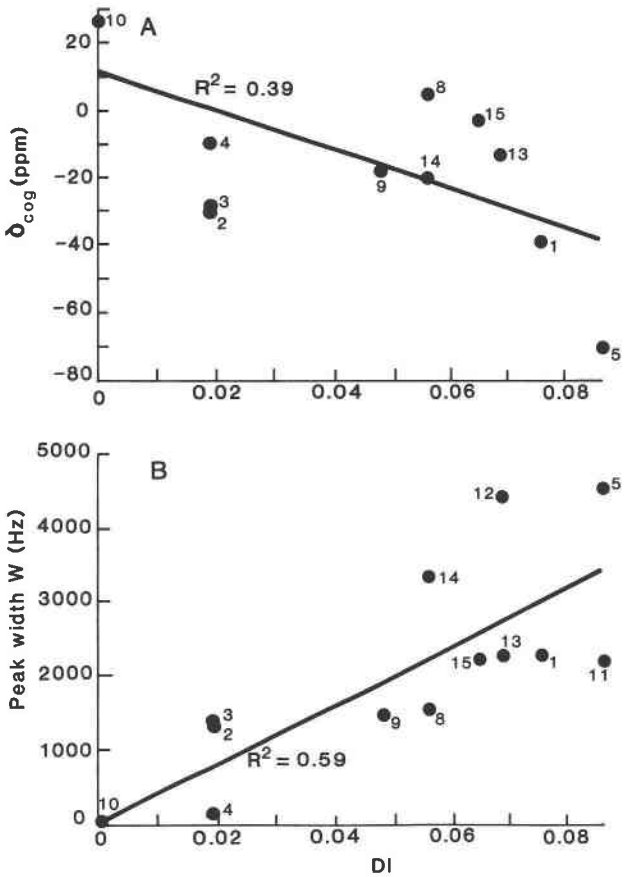

Fig. 7. Relation between the octahedral angular *DI* of Mg-bearing minerals and (**A**) the center of gravity of the observed ^{25}Mg resonance positions, δ_{cog}, and (**B**) the observed resonance widths at half height. Regression line fitted to all points. Key: 1 = brucite, 2 = magnesite, Canada, 3 = magnesite, Antarctica, 4 = dolomite, 5 = hydrotalcite, 6 = hydromagnesite M1, 7 = hydromagnesite M2, 8 = talc, 9 = enstatite, 10 = periclase, 11 = forsterite M1, 12 = forsterite M2, 13 = antigorite, 14 = montmorillonite, 15 = phlogopite. Widths for forsterite calculated from the data of Derighetti et al. (1978).

data (Hazen, 1976) indicate that both octahedral sites are significantly distorted (Table 3). A previous single-crystal ^{25}Mg NMR study of forsterite (Derighetti et al., 1978) reported values of χ of 4.996 and 4.313 MHz and values of η of 0.963 and 0.396 for the M1 and M2 sites, respectively, leading to the simulated MAS spectra shown in Figure 6B. Although the simulated resonance for the more distorted M1 site is quite different from that recorded for heated chrysotile, the simulated M2 resonance bears some similarity to the observed spectrum, in terms of the quadrupolar separation and resonance width. However, on the basis of these results it is impossible to determine whether the observed resonance is related to the less distorted site in forsterite, or whether it arises from a few percent of some X-ray amorphous impurity with an NMR spectrum fortuitously similar to that of the M2 site of forsterite. Forsterite might not be observed under the present experimental conditions, since the EFG-broadening would reduce the signal height to only a few percent of a single peak not EFG-broadened. A further possibility is that forsterite has a long ^{25}Mg T_1.

Periclase, MgO. The [6]Mg site in periclase is regular, with a *DI* of 0. The ^{25}Mg MAS NMR spectrum (Fig. 3F) consists of a single extremely narrow resonance with a chemical shift (26.5 ppm) in good agreement with that previously reported by Dupree and Smith (1988).

Spinel, $MgAl_2O_4$. Attempts were made to record the MAS NMR spectrum from several spinel samples, including materials synthesized from the pure oxides at 1300 °C for 128 h and by heating synthetic hydrotalcite at 1300 °C for 19.5 h together with a natural sample from Amity, New York (sample NZGS 53759). The ^{27}Al MAS NMR spectrum of the spinel from hydrotalcite indicated an inversion parameter $x = 0.32$, whereas the natural spinel contained virtually no [4]Al, consistent with a fully ordered material. Although all of these samples have the XRD pattern of crystalline spinel, none of them showed the single resonance reported at 52 ppm by Dupree and Smith (1988) in an undescribed spinel sample. Even with a recycle delay of 60 s, no ^{25}Mg resonance at all was detected in the synthetic samples, other than a small MgO signal, which had a T_1 of a few seconds. The natural sample showed a much more complex spectrum than that of Dupree and Smith (1988) and will be the subject of further investigation.

Effects of octahedral site distortions on the ^{25}Mg NMR spectra

It is clear from the forgoing discussion and spectral simulations that the shape and position of these ^{25}Mg mineral spectra, where Mg is in its preferred octahedral coordination, is dominated by EFG effects. In minerals, these are influenced by a number of factors, including the nature of the species in the first coordination sphere (O, OH, CO_3, H_2O) and in the next coordination sphere (other species such as Si, Al, Fe, and exchangeable cations) and geometrical effects such as the flattening of the octahedral layer or curling of the sheets to relieve mismatch between the octahedral and tetrahedral sheets of layer structures.

A variety of parameters have been suggested for estimating the relative degree of distortion around an octahedral site, based both on octahedral bond lengths and angles. The present data were tested against two angle-based parameters, the simplest being the angular *DI* of Baur (1974):

$$DI = \left(\sum_{i=1}^{12} |\Theta_i - \Theta_m| \right) \Big/ 12\Theta_m \qquad (1)$$

where Θ_i and Θ_m are the observed and true (undistorted) octahedral angles, respectively. The other angular relationship tested here was suggested by Ghose and Tsang (1973) to be related to the nuclear quadrupole coupling constant χ and is essentially a measure of the shear strain ψ within the coordination polyhedra, defined as

$$\Psi = \sum_i |\tan(\Theta_i - \Theta_m)|. \quad (2)$$

Of the bond-length relationships tested against the present spectral data, the simplest is the mean octahedral bond length l_m, defined as

$$l_m = \tfrac{1}{6} \sum_i l_i \quad (3)$$

where l_i are the individual octahedral bond lengths. By analogy with ^{29}Si chemical shifts, the mean bond length l_m might be expected to correlate with δ_0, the chemical shift corrected for EFG effects. Another bond-length relationship, suggested by Ghose and Tsang (1973) to correlate with χ, is the longitudinal strain α, defined as

$$\alpha = \sum_i |\ln(l_i/l_m)| \quad (4)$$

where l_m is the mean octahedral Mg-O length. The relevant bond lengths and angles were computed from the crystallographic data using the program of Larson et al. (1991). The various structural parameters computed for the minerals of the present suite for which crystallographic data are available are presented in Table 3.

Although the complexity of EFG effects renders it unlikely that a simple relationship between EFG-related parameters and structural distortions of the first coordination sphere will exist for all compounds, the utility of this approach was considered to be worth investigating.

In the first instance, simple relationships were sought between the octahedral *DI* (Eq. 1) and the two most readily measured spectral parameters, δ_{cog}, the position of the peak center of gravity (determined by integration of the resonance) and *W*, the width of the resonance at half its height, since δ_{cog} should shift upfield and *W* increase as the EFG increases. A relationship between δ_{cog} and *DI* does appear to exist (Fig. 7A), but the scatter in this graph suggests that, as expected, factors other than EFG effects influence the position of the resonance. It was noted that if the data for the carbonate minerals are omitted, the correlation coefficient is improved to 0.67. The plot of *W* vs. *DI* (Fig. 7B) also shows a better linear relationship to all the data points, suggesting that this parameter may be more directly related to the EFG.

For samples in which reasonably reliable nuclear quadrupole coupling constants χ could be derived from the spectral simulations (Table 2), this parameter might also be expected to show a relationship with structural distortion parameters such as *DI* and ψ. The minerals for which the calculated χ values were deemed to be the most reliable were brucite, magnesite, dolomite, hydrotalcite, and periclase. Also included are the χ values of the M1 and M2 sites of forsterite, from Derighetti et al. (1978). A plot of these values of χ vs. ψ, as defined by Equation 2, has a correlation coefficient of 0.82 and passes close to the origin (Fig. 8A).

Figure 8B shows the analogous plot for χ vs. *DI*, in which the regression line is again fitted only to the data

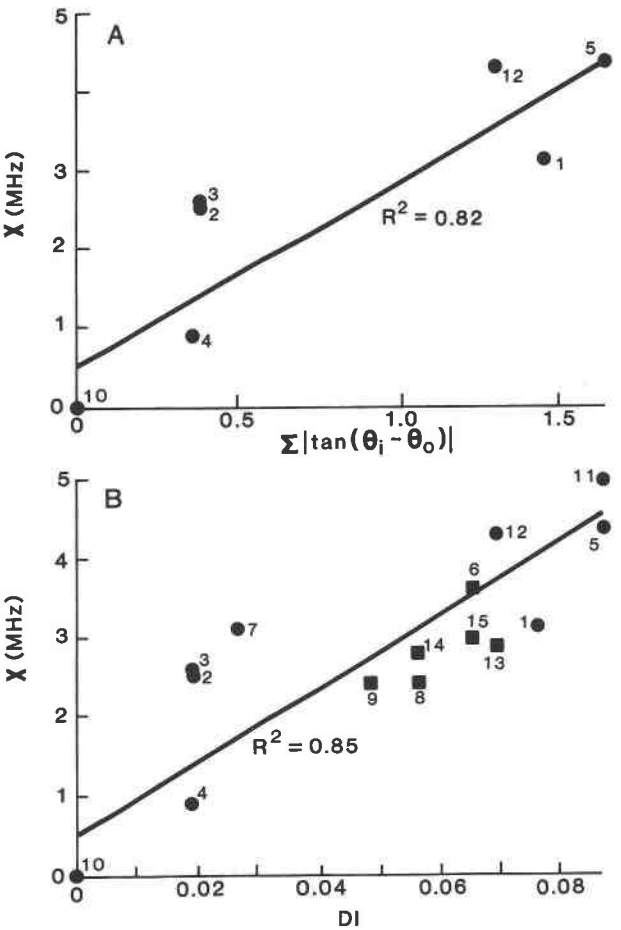

Fig. 8. Relation between the nuclear quadrupole coupling constant χ derived from the spectral simulations and functions describing the octahedral angular distortion. (**A**) Plotted as a function of polyhedral shear strain, most reliable χ data only, points numbered as for Fig. 7. Regression line fitted to all points. (**B**) Plotted as a function of the angular *DI*, most reliable χ data denoted by solid circles, other estimates of χ, denoted by solid squares, included for interest. Regression line fitted to most reliable data only. Points numbered as for Fig. 7. Data for forsterite taken from Derighetti et al. (1978).

points embodying the reliable values of χ (denoted by solid circles). However, also included on this graph are data points for the samples that showed featureless spectra and for which only the range of χ values could be deduced (solid squares); although the points plotted here are the maximum values of χ, which can range down to 0, their closeness to the regression line in most cases indicated that the χ values of these minerals are probably nonzero and may lie close to the maximum estimated value.

Relationships were also sought with geometrical functions based on octahedral bond lengths. The correlation between χ and longitudinal strain α (Eq. 4), predicted by Ghose and Tsang (1973) could not be found, even for the most reliable χ data, nor was a correlation found between

χ and the simpler bond-length parameter Δl, the difference between the maximum and minimum bond lengths. There are insufficient accurate data to test the expected relationship between l_m and the corrected chemical shift δ_0.

Thus, of all the relationships tested, the best correlations were found between the most reliable values of χ and functions describing distortions of the octahedral bond angles (*DI* or ψ). Although EFG effects are likely to be more complex than what is suggested by these simple relationships (as evidenced by the effect of substituting carbonate for oxide or hydroxide groupings), these distortion relationships provide a simple means of tentatively assigning resonances to specific sites or possibly even predicting the spectrum of a new compound.

Acknowledgments

We are indebted to L. Groat, University of British Columbia, P.J. Dunn, Smithsonian Institution, and W. Waters, N.Z. Geological Survey, for providing some of the samples, to K. Card and R. Goguel for the chemical analyses, and to G.J. Gainsford for helpful crystallographic discussions.

References cited

Akao, M., Marumo, F., and Iwai, S. (1974) The crystal structure of hydromagnesite. Acta Crystallographica, B30, 2670–2672.

Allmann, R., and Jepsen, H.P. (1969) Die Struktur des Hydrotalkits. Neues Jahrbuch für Mineralogie Monatshefte, 12, 544–551.

Bastow, T.J. (1991) ^{25}Mg nuclear quadrupole coupling in $Mg(OH)_2$. Solid State Communications, 77, 547–548.

Baur, W.H. (1974) The geometry of polyhedral distortions: Predictive relationships for the phosphate group. Acta Crystallographica, B30, 1195–1215.

Derighetti, B., Hafner, S., Marxer, H., and Rager, H. (1978) NMR of ^{29}Si and ^{25}Mg in Mg_2SiO_4 with dynamic polarization technique. Physics Letters, 66A, 150–152.

Dupree, R., and Smith, M.E. (1988) Solid-state magnesium-25 NMR spectroscopy. Journal of the Chemical Society, Chemical Communications, 1483–1485.

Ghose, S., and Tsang, T. (1973) Structural dependence of quadrupole coupling constant e^2qQ/h for ^{27}Al and crystal field parameter D for Fe^{3+} in aluminosilicates, American Mineralogist, 58, 748–755.

Guven, N., Caillerie, J-B.E., and Fripiat, J.J. (1992) The coordination of aluminium ions in the palygorskite structure. Clays and Clay Minerals, 40, 457–461.

Hazen, R.M. (1976) Effects of temperature and pressure on the crystal structure of forsterite. American Mineralogist, 61, 1280–1293.

Hazen R.M., and Burnham, C.W. (1973) The crystal structures of one-layer phlogopite and annite. American Mineralogist, 58, 889–900.

Jones, B.F., and Galan, E. (1988) Sepiolite and palygorskite. In Mineralogical Society of America Reviews in Mineralogy, 19, 631–674.

Kirkpatrick, R.J. (1988) MAS NMR spectroscopy of minerals and glasses. In Mineralogical Society of America Reviews in Mineralogy, 18, 341–403.

Kunze, G. (1958) Die gewellte Struktur des Antigorits, I. Zeitschrift für Kristallographie, 110, 282–320.

Larson, A.C., Lee, F.L., LePage, Y., Webster, M., Charland, J.P., White, P.S., and Gabe, E. (1991) NCRVAX: The NCRVAX crystal structure system. Chemistry Division, NRC, Ottawa, Canada K1A OR6.

MacKenzie, K.J.D., and Meinhold, R.H. (1993a) A 25-Mg MAS NMR study of the thermal decomposition of magnesium carbonate. Journal of Materials Science Letters, 12, 1696–1698.

——— (1993b) Thermal decomposition of dolomite, calcium magnesium carbonate, studied by 25-Mg solid state nuclear magnetic resonance. Thermochimica Acta, in press.

——— (1994) Thermal reactions of chrysotile revisited: A ^{29}Si and ^{25}Mg MAS NMR study. American Mineralogist, 79, 43–50.

Markgraf, S.A., and Reeder, R.J. (1985) High-temperature structure refinements of calcite and magnesite. American Mineralogist, 70, 590–600.

Mellini, M. (1982) The crystal structure of lizardite *1T*: Hydrogen bonds and polytypism. American Mineralogist, 67, 587–598.

Mellini, M., and Zanazzi, P.F. (1987) Crystal structures of lizardite-*1T* and lizardite-$2H_1$ from Coli, Italy. American Mineralogist, 72, 943–948.

Morimoto, N., and Koto, K. (1969) The crystal structure of orthoenstatite. Zeitschrift für Kristallographie, 125, 65–83.

Oh, K.D., Morikawa, H., Iwai, S., and Aoki, H. (1973) The crystal structure of magnesite. American Mineralogist, 58, 1029–1033.

Ohashi, Y. (1984) Polysynthetically-twinned structures of enstatite and wollastonite. Physics and Chemistry of Minerals, 10, 217–229.

Perdikatsis, B., and Burzlaff, H. (1981) Strukturverfeinerung am Talk $Mg_3[(OH)_2Si_4O_{10}]$. Zeitschrift für Kristallographie, 156, 177–186.

Rayner, J.H. (1974) The crystal structure of phlogopite by neutron diffraction. Mineralogical Magazine, 39, 850–856.

Rayner, J.H., and Brown, G. (1973) The crystal structure of talc. Clays and Clay Minerals, 21, 103–114.

Reeder, R.J., and Wenk, H.-R. (1983) Structure refinements of some thermally disordered dolomites. American Mineralogist, 68, 769–776.

Sanz, J., and Stone, W.E.E. (1979) NMR study of micas. II. Distribution of Fe^{2+}, F^- and OH^- in the octahedral sheet of phlogopites. American Mineralogist, 64, 119–126.

Tsipursky, S.I., and Drits, V.A. (1984) The distribution of octahedral cations in the 2:1 layers of dioctahedral smectites studied by oblique-texture electron diffraction. Clay Minerals, 19, 177–193.

Whittaker, E.J.W. (1956) The structure of chrysotile. II. Clino-chrysotile. Acta Crystallographica, 9, 855–864.

Wicks, F.J., and O'Hanley, D.S. (1988) Serpentine minerals: Structures and petrology. In Mineralogical Society of America Reviews in Mineralogy, 19, 91–167.

Zhang, S., Wu, X., and Mehring, M. (1990) Elimination of ringing effects in multiple-pulse sequences. Chemical Physics Letters, 173, 481–484.

Zigan, F., and Rothbauer, R. (1967) Neutronenbeugungsmessungen am Brucit. Neues Jahrbuch für Mineralogie Monatshefte, 4/5, 137–143.

Manuscript received July 22, 1993
Manuscript accepted November 18, 1993